Expression and one-step purification of active LPL contemplated by biophysical considerations
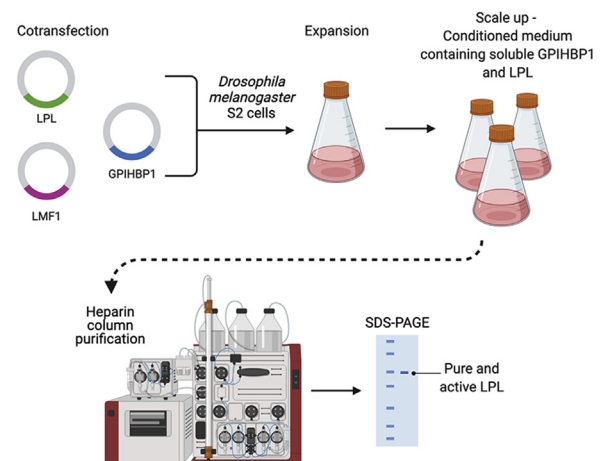
Anne-Marie Lund Winther[1,2]*[iD] , Kristian Kølby Kristensen[1,2][iD] , Anni Kumari[1,2][iD] , and Michael Ploug[1,2][iD]

[1]Finsen Laboratory, Rigshospitalet, Copenhagen, Denmark; and [2]Biotech Research and Innovation Centre, University of Copenhagen, Copenhagen, Denmark

Abstract LPL is essential for intravascular lipid metabolism and is of high medical relevance. Since LPL is notoriously unstable, there is an unmet need for a robust expression system producing high quantities of active and pure recombinant human LPL (hLPL). We showed previously that bovine LPL purified from milk is unstable at body temperature (T_m is 34.8°C), but in the presence of the endothelial transporter glycosylphosphatidylinositol-anchored high density lipoprotein-binding protein 1 (GPIHBP1), LPL is stabile (T_m increases to 57.6°C). Building on this information, we now designed an expression system for hLPL using *Drosophila* Schneider 2 cells grown in suspension at high cell density and at an advantageous temperature of 25°C. We cotransfected Schneider 2 cells with hLPL, lipase maturation factor 1, and soluble GPIHBP1 to provide an efficient chaperoning and stabilization of LPL in all compartments during synthesis and after secretion into the conditioned medium. For LPL purification, we used heparin-Sepharose affinity chromatography, which disrupted LPL-GPIHBP1 complexes causing GPIHBP1 to elute with the flow-through of the conditioned media. This one-step purification procedure yielded high quantities of pure and active LPL (4–28 mg/l). Purification of several hLPL variants (furin cleavage-resistant mutant R297A, active-site mutant S132A, and lipid-binding-deficient mutant W390A-W393A-W394A) as well as murine LPL underscores the versatility and robustness of this protocol. Notably, we were able to produce and purify LPL containing the cognate furin cleavage site. ⬛ This method provides an efficient and cost-effective approach to produce large quantities of LPL for biophysical and large-scale drug discovery studies.

Created with BioRender.com

LPL is synthesized by myocytes and adipocytes and secreted into the subendothelial spaces where it becomes transiently tethered to heparan sulfate proteoglycans before it translocates to its site of action in the capillary lumen (1). The obligate binding partner of LPL, the glycosylphosphatidylinositol-anchored high density lipoprotein-binding protein 1 (GPIHBP1), mediates the bidirectional transcytosis of LPL across the endothelium (2). On the luminal surface of the capillary membrane, the LPL·GPIHBP1 complex is responsible for the margination of circulating triglyceride-rich lipoproteins (chylomicrons or very low density lipoproteins) and for the subsequent triglyceride hydrolysis releasing free fatty acids—the energy source for nearby vital tissues, for example, heart, skeletal muscle, and brown adipose tissue (3). When this lipolysis platform is dysfunctional, because of loss-of-function variants in *LPL* or *GPIHBP1* (4) or to the presence of neutralizing GPIHBP1 autoantibodies (5), the affected individuals develop severe hypertriglyceridemia with increased risk of acute pancreatitis. This relationship prompted intense research on the development of clinical intervention strategies aimed at lowering plasma triglyceride levels by promoting the efficiency of this intravascular lipolysis platform. One strategy focuses on reducing the repression from the natural LPL inhibitors angiopoietin-like proteins 3, 4,

*For correspondence: Anne-Marie Lund Winther, Anne.Marie@finsenlab.dk.

and 8 (6–8). These interventions are not effective in patients with monogenic familial LPL deficiency (9), who would likely benefit from an exogenous supply of LPL by enzyme replacement therapy with purified and stable LPL protein or by *LPL* gene therapy (10).

In a historical perspective, most of the pioneering studies on structure-function relationships in LPL used bovine LPL (bLPL) purified from cow milk in large quantities (11). Unfortunately, efforts to purify endogenous hLPL from human postheparin plasma only produced minute amounts of highly unstable hLPL (10 µg/l) (12). Studies on human LPL (hLPL) had to rely on postheparin plasma or culture media harvested from transfected cells secreting moderate amounts of recombinant LPL (13–17).

Several protocols for recombinant LPL expression and purification have been published in an attempt to meet the demands for large amounts of purified, active, and homogenous LPL (in milligram quantities) to conduct contemporary biophysical experiments, such as X-ray crystallography, small-angle X-ray scattering, and hydrogen-deuterium exchange MS. A recent study used Flp-In™T-Rex™ human embryonic kidney 293 adherent cells that were cotransfected with lipase maturation factor 1 (LMF1) and hLPL^{R297N}, where a neoglycosylation site in hLPL was introduced at position 297 to minimize undesired furin cleavage during production (18). This protocol yielded however only approximately 0.1 mg hLPL per liter culture medium. Two biopharmaceutical companies have independently reported large-scale purifications of hLPL and used those preparations to solve the first crystal structure of LPL. Shire (Cambridge, MA) used modified proprietary Chinese hamster ovary cells cotransfected with hLMF1 and hLPL^{R297A} (furin-resistant LPL mutant) to produce >20 mg of hLPL per liter culture medium (19). Novartis (Cambridge, MA) used human embryonic kidney 293-F suspension cells that coexpressed a His-tagged hLPL, LMF1, and GPIHBP1 to obtain 6 mg hLPL·hGPIHBP1 complexes per liter of culture media (20, 21). In this study, we designed an easily accessible and robust protocol for the large-scale production and purification of milligram quantities of recombinant hLPL in the absence of bound ligands. Building on our recent knowledge on bLPL stability and intracellular chaperoning during de novo biosynthesis of hLPL (22–24), we reasoned that stabilization of LPL in all compartments of its production and purification would greatly enhance the performance of such a production platform. The key features of the present protocol are *i*) a lowering of the temperature for the cell culture conditions (25 vs. 37°C) to minimize thermal unfolding of LPL (23); *ii*) the coexpression of LMF1 to assist folding of LPL in the endoplasmic reticulum (25, 26); and *iii*) the coexpression of a soluble version of GPIHBP1 to stabilize LPL in all compartments (27), to minimize furin-mediated cleavage (28), and to act as a surrogate for syndecan-1 during *trans*-Golgi sorting and secretion (24). A one-step purification from the conditioned medium (CM) using heparin-Sepharose yielded highly pure and active LPL without GPIHBP1. We demonstrate the robustness and versatility of this protocol by producing pure and active hLPL (including several mutants thereof) as well as active mouse LPL (mLPL)—all in quantities ranging from 4 to 28 mg/l culture media.

MATERIALS AND METHODS

Reagents

The *Drosophila melanogaster* Schneider 2 (S2) cells, pCoHY-GRO, Cellfectin II reagent, Schneider's Drosophila medium, Express-Five serum-free medium (SFM), and Hygromycin B were all from Thermo Fisher Scientific. Monoclonal antibodies 5D2 and R2 were produced and characterized as described (29, 30). bLPL was purified from fresh bovine milk (11) and kindly provided by Dr Gunilla Olivecrona (Umeå University, Sweden).

Expression and purification of hLPL

We purchased LPL, LMF1, and GPIHBP1 constructs from VectorBuilder, Inc. The mature part of hLPL (NM_000237.2) covering residues 1–448 was inserted into the pMT/V5-His vector with an N-terminal BiP signal sequence (**Fig. 1**). hLPL carried a R297A mutation to avoid furin cleavage at the furin recognition motif RAKR (numbering starting from the first amino acid in the mature LPL). hLMF1 (NM_022773.3) was inserted into the pMT vector with an N-terminal 6xHis-tag and a tobacco etch virus cleavage site. An N-terminal 6xHis-tag was included in the construct to enable later verification of LMF1 expression in the transfected S2 cells using Western blots developed with an anti-His-antibody. Soluble hGPIHBP1 (EAW82276.1) covering residues 1–131 was constructed with a R38G mutation (numbering starting from the first amino acid in the mature GPIHBP1) and the human suPAR-DIII^{R281G} domain in front as purification tag (31) followed by an enterokinase cleavage site and purified as described (27). hGPIHBP1 refers to this soluble truncated protein throughout the article.

The hLPL$^{R297A-W390A-W393A-W394A}$ construct was prepared using the hLPL^{R297A} template and QuickChange II site-directed mutagenesis kit (Agilent Technologies; catalog no.: 200523) with primer: 5′-GATTCATACTTTAGCG CGTCAGACGCGGCGAGCAGTCCCGGCTTCG-3′, whereas hLPL$^{S132A-R297A}$ was produced using primer: 5′-CTCTT GGGATACGCCCTTGGAGCCCATG-3′.

hLPL wt was obtained using the hLPL^{R297A} template and primer: 5′-GTCAGAGCCAAGAGAAGCAGCAAAATGTAC CTGAAGACTCG-3′.

The mature part of mLPL (CT010344) covering residues 1–447 was inserted into the pMT vector with a BiP signal sequence and a R297A mutation (Fig. 1). mLPL construct was obtained using the mLPL^{R297A} template and primer: 5′-CAAGGTCAGAGCCAAGAGAAGCAGCAAGATGTA CCTG-3′. mLMF1 (NM_029624.4) were inserted in the pMT vector with an N-terminal 6xHis-tag and a tobacco etch virus cleavage site. Soluble mGPIHBP1 (NM_026730) covering residues 1–176 were constructed with a R34G mutation and with a human suPAR-DIII^{R281G} tag similar to that described for hGPIHBP1 (27).
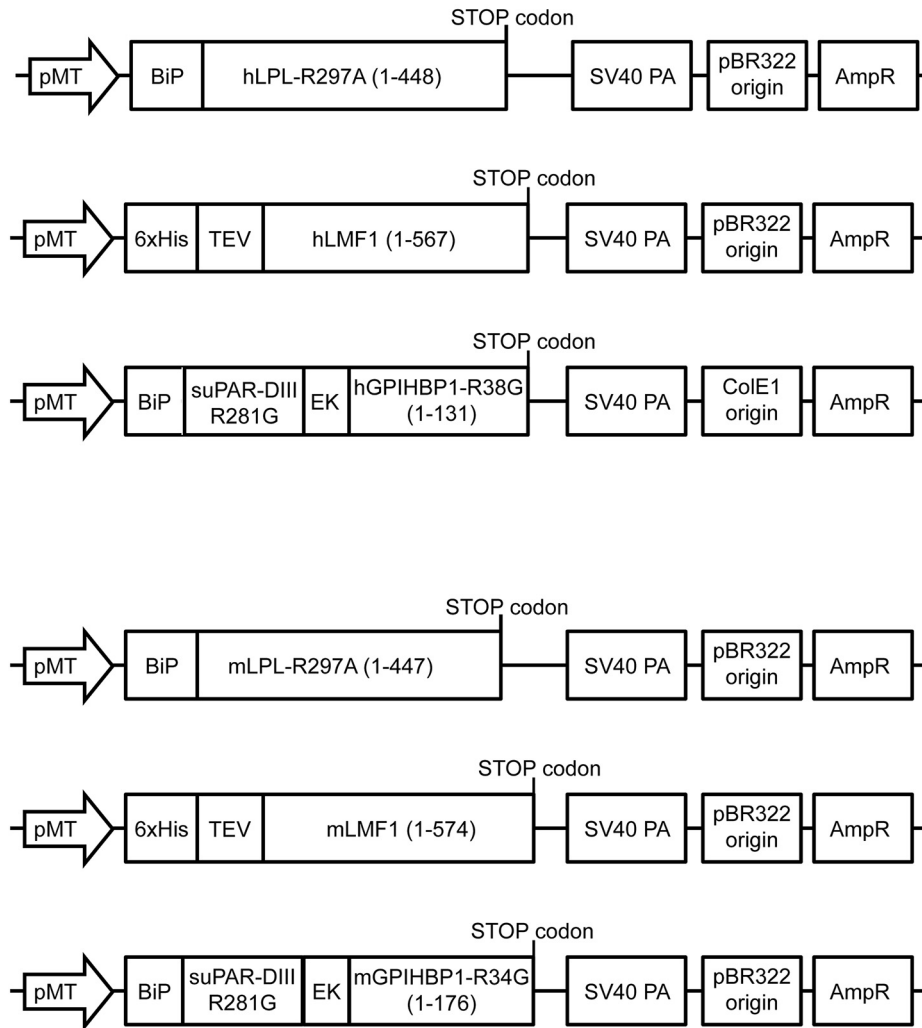
Fig. 1. Vector constructs of LPL, LMF1, and GPIHBP1 for expression in *Drosophila melanogaster* S2 cells. The sequences for hLPL^{R297A} (residues 1–448) and mLPL^{R297A} (residues 1–447) were inserted into the pMT/V5-His vector with a BiP signal sequence. Downstream of a Simian virus 40 polyadenylation signal sequence (SV40 PA), a pBR322 origin that facilitate replication in *Escherichia coli* and an ampicillin-resistant (AmpR) protein is inserted. Full-length LMF1 was inserted in a pMT/V5-His vector with an N-terminal 6xHis tag and tobacco etch virus protease cleavage site. The soluble domain of GPIHBP1 was positioned with an N-terminal BiP signal sequence and a suPAR-DIII(R281G) purification tag followed by an enterokinase cleavage site (EK) in the pMT/V5-His vector.

Initially, four different hLPL expression cell lines were produced by stable transfection of 3×10^6 cells/ml *Drosophila* S2 cells in 3 ml SFM with *i*) 6 µg hLPL^{R297A}; *ii*) 6 µg hLPL^{R297A} and hGPIHBP1 in 1:1 w/w ratio; *iii*) 6 µg hLPL^{R297A} and 1.5 µg hLMF1 in a 4:1 w/w ratio, or *iv*) 6 µg hLPL^{R297A}, 3 µg hGPIHBP1 and 1.5 µg hLMF1 in a 4:2:1 w/w ratio. Transfections of *v*) 6 µg hLPL, *vi*) 6 µg hLPL$^{R297A-W390A-W393A-W394A}$, or *vii*) 6 µg hLPL$^{S132A-R297A}$ were all performed with 3 µg hGPIHBP1 and 1.5 µg hLMF1 in a 4:2:1 w/w ratio. Likewise, transfection with mLPL was performed with 6 µg mLPL^{R297A} (or mLPL), 3 µg mGPIHBP1, and 1.5 µg mLMF1. Cellfectin II reagent was used for all transfections, and 0.6 µg pCoHYGRO was added as selection plasmid. Selection of transfected cells was accomplished by growing the cells at 25°C in Schneider's Drosophila medium in the presence of 300 µg/ml hygromycin B for 3–4 weeks.

For protein expression and purification, transfected cells were transferred to SFM, and after 7 days of induction with 0.5 mM CuSO$_4$, CM was harvested and supplemented with 0.1 volume of 1 M Tris-HCl (pH 8), 0.2 M EDTA, 0.01% Triton X-100, and finally 0.005 volumes of 200 mM PMSF dissolved in DMSO, the latter addition occurred under rigorous stirring. Addition of 20 mM EDTA at pH 8 to the CM was found empirically to prolong the expected half-lives of our affinity columns by lowering the risk of column clotting—one likely explanation is that it reduces protein precipitation by the Cu^{2+} added to the medium to induce protein expression ([31], [32]). Addition of 1 mM PMSF to the CM reduced the risk of proteolytic degradation of LPL during heparin-Sepharose purification. Under these conditions, we observed no covalent modification of the active site serine in the purified LPL as assessed by tryptic MALDI-MS peptide profiling. Before affinity purification, the CM were filtrated (0.2 µm pore sizes) and then applied to a 1 ml HiTrap heparin affinity column (Cytiva) equilibrated with buffer A (0.4 M NaCl, 10 mM Bis-Tris [pH 6.5], 10% glycerol) at 4°C and washed with buffer A containing 0.9 M NaCl until absorbance at 280 nm reached baseline (usually a 25 ml washing step). A 12 ml gradient from 0.9 M NaCl to 2 M NaCl in buffer A eluted the bound LPL with a flow of 0.4 ml/min and subsequent analyses with 12%

Bis-Tris SDS-PAGE gels (NuPAGE, Thermo Fisher Scientific) identified the relevant fractions. Pure LPL fractions were pooled and concentrated by ammonium sulfate precipitation (33). To retain LPL activity, this was performed by dialyzing the pooled sample into 3.6 M $(NH_4)_2SO_4$ and 50 mM Bis-Tris (pH 6.5) at 4°C. Precipitation of LPL was visible after 3–5 h and collected by centrifugation at 15,000 g, 15 min, at 4°C. The pellet was resuspended in 10 mM Tris-HCl (pH 7.2), 0.15 M NaCl, 10% glycerol or 10 mM Tris-HCl (pH 7.2), 1 M NaCl, and 40% glycerol (33).

Western blot

Samples containing 0.3 μg hLPL were analyzed using 12% Bis-Tris SDS-PAGE gels and transferred to PVDF membranes. The membranes were blocked 1 h and then probed with 0.5 μg/ml of the monoclonal 5D2 antibody in PBS with 5% skimmed milk and 0.2% Tween-20 for LPL detection. The monoclonal antibody R2, which recognizes the suPAR-DIII purification tag located in front of hGPIHBP1, was used to visualize GPIHBP1 by incubating the blotted PVDF membrane with 0.4 μg/ml R2 in PBS with 2% BSA and 0.2% Tween-20. After washing, the PVDF membranes were incubated 1 h with secondary antibody IRDye800CW goat anti-mouse (LI-COR Biosciences; catalog no.: 926-32210) in 1:10,000 ratio, and after washing, the blot was scanned using an Odyssey Infrared Scanner (LI-COR Biosciences).

Furin cleavage

hLPL^{R297A}, hLPL, mLPL^{R297A}, and mLPL were subjected to furin cleavage by incubating 10 μM purified LPL with 4U furin (Sigma-Aldrich; catalog no.: F2677-50UN) in 10 mM MES, 1 mM CaCl$_2$, and 0.15 M NaCl (pH 7.0) for 0 and 120 min at 25°C with shaking (560 rpm). The samples were prepared for SDS-PAGE (reduced and alkylated), and the degree of furin cleavage was assessed by SDS-PAGE using 12% Bis-Tris SDS-PAGE gels.

MS

Purified LPL preparations were analyzed by a Bruker autoflex maX MALDI-TOF MS operating in positive linear mode. Samples of 0.2 mg/ml LPL were desalted by binding to a ZipTip$_{C4}$ (Millipore; catalog no.: ZTC04S096) and 1 μl eluted directly on the stainless steel target plate with 1 μl of 10 mg/ml α-cyano-4-hydroxycinnamic acid dissolved in 50% acetonitrile and 5% formic acid.

Lipase activity assay

To determine lipase activity, 90 μl incubation mixtures containing 166 mM NaCl, 28 U/ml heparin, 10% (w/v) serum albumin fatty acid free (Sigma-Aldrich; catalog no.: 10775835001), 250 mM Tris-HCl (pH 8.5), 0.16% intralipid (Sigma-Aldrich; catalog no.: I141), and 6% chicken serum (Sigma-Aldrich; catalog no.: C5405) were mixed with 60 μl of sample buffer consisting of 150 mM NaCl, 0.1% serum albumin fatty acid free, 0.01% Triton X-100, 10 mM Hepes (pH 7.4), and 10 nM LPL. Serum albumin was added to immobilize excess free fatty acids released during lipolysis that would otherwise cause product inhibition of LPL activity (34). Chicken serum was added as a source of cofactor of LPL apoC-II and heparin-stabilized LPL. After 25 min of incubation, nonesterified fatty acids (NEFAs) released by LPL were

quantified using the NEFA-HR kit according to the manufacturer's protocol (Wako Chemicals). The specific activity of the different batches was determined in the presence of GPIHBP1 in a 1:1 ratio. To optimize storage conditions for the activity of purified LPL, it was stored at 1 mg/ml at three different conditions: *i*) 0.2 M NaCl, 10 mM Tris-HCl (pH 7.2); *ii*) 0.2 M NaCl, 10 mM Tris-HCl (pH 7.2), 40% glycerol; and *iii*) 1.2 M NaCl, 10 mM Tris-HCl (pH 7.2), 40% glycerol for various times at 23, 4, −20, and −80°C.

Esterase activity assay

The triglyceride derivative 1,2-di-O-lauryl-rac-glycero-3-glutaric acid (6′-methylresorufin) ester (DGGR) assay (35) was used to determine the esterase activity of hLPL, hLPL^{R297A}, hLPL$^{R297A-W390A-W393A-W394A}$, hLPL$^{S132A-R297A}$, mLPL, mLPL^{R297A}, and bLPL. In brief, 2-fold serial dilutions of LPL (30 –3.8 nM) in assay buffer (50 mM Tris-HCl [pH 7.2], 120 mM NaCl, 10 mg/ml serum albumin fatty acid free, and 0.5% Triton X-100 [v/v]) was incubated with 20 μM DGGR substrate for 20 min at 25°C. Incubations were conducted in black 96-well plates in a total volume of 100 μl. The formation of methylresorufin was measured at 615 nm upon excitation at 535 nm using a PerkinElmer Envision plate reader.

Surface plasmon resonance

Real-time binding kinetics for the LPL·GPIHBP1 interaction was measured by a BiacoreT200™ essentially as described (36). In brief, we immobilized the anti-LPL monoclonal antibody 5D2 (29), which recognized the Trp-rich lipid-binding loop of LPLs (37), as capture antibody on a CM4 sensor chip. The kinetics of the LPL$^{R297A-W390A-W393A-W394A}$ mutant was unfortunately not amenable by this protocol, since 5D2 is able to capture neither this particular hLPL variant nor mLPL. To ensure LPL stability during the capture procedure, we used a 10 mM Hepes (pH 7.4) buffer including 300 mM NaCl, 4 mM CaCl$_2$, 10% (v/v) glycerol, 0.05% (v/v) surfactant P20, 1 mg/ml serum albumin fatty acid free, 0.1 mg/ml carboxylmethyl dextran, and 0.05% (w/v) NaN$_3$. To minimize LPL unfolding during the surface plasmon resonance (SPR) analyses, we used a single cycle protocol for the real-time binding by injecting five serial 2-fold dilutions of a truncated and soluble human GPIHBP1 (27) ranging from 0.5 to 8 nM. The running buffer was 10 mM Hepes (pH 7.4), 150 mM NaCl, 4 mM CaCl$_2$, 0.05% (v/v) P20, 0.2 mg/ml defatted BSA, and 0.05% (w/v) NaN$_3$. After double-buffer referencing, we determined the binding rate constants (k_{on} and k_{off}) for the LPL·GPIHBP1 interaction by fitting the data to a simple bimolecular interaction model with the mathematical model developed for single-cycle kinetics (T200 Evaluation Software 3.0; GE Healthcare).

Native PAGE gel

Samples of 2 μM hLPL, hLPL$^{R297A-W390A-W393A-W394A}$, or mLPL were preincubated for 30 min on ice with or without 12 μM hGPIHBP1. To measure the interaction with lipids, hLPL·hGPIHBP1 and hLPL$^{R297A-W390A-W393A-W394A}$·hGPIHBP1 complexes were incubated in the absence or the presence of a 0.25% intralipid suspension. All samples were loaded on 4–16% native polyacrylamide gels and subjected to a field gradient of 100 V for 10 min, 200 V for 30 min, and 300 V for 20 min at 4°C in a Tris-glycine buffer. The gel was stained with Coomassie G-250 to visualize the protein migration pattern.

TABLE 1. Comparison of purification yields and specific lipase and esterase activities of hLPL produced under different expression conditions

Expression condition	Yield of LPL (mg/l)[a]	Specific lipase activity of LPL (U/mg)[a]	Specific esterase activity of LPL (RFU/min/nM)[b]	LPL Mass[MS], Da (Δmass)[c]
hLPL-R297A	0.3	No activity	No activity	ND
hLPL-R297A + hGPIHBP1	0.7	131 ± 8	94 ± 8	52,535 (+147)
hLPL-R297A + hLMF1	2.2	90 ± 31	68 ± 3	52,593 (+205)
hLPL-R297A + hGPIHBP1 + hLMF1	13.5	138 ± 16	92 ± 14	52,593 (+205)
hLPL-R297A-W390A-W393A-W394A + hGPIHBP1 + hLMF1	3.7	No activity	13 ± 1	52,020 (−23)
hLPL-S132A-R297A + hGPIHBP1 + hLMF1	4.7	No activity	No activity	52,623 (+235)
hLPL + hGPIHBP1 + hLMF1	28.2	141 ± 48	109 ± 15	52,262 (−211)
mLPL-R297A + mGPIHBP1 + mLMF1	7.4	178 ± 61	98 ± 9	52,319 (+11)
mLPL + mGPIHBP1 + mLMF1	8.4	140 ± 33	110 ± 14	52,433 (+40)
bLPL	—	285 ± 26	130 ± 7	53,875 (−)

ND, not determined.
[a]Average values of three to six independent LPL purifications are shown for each variant.
[b]Mean and standard derivations are calculated from three replicates of each given LPL variant.
[c]Δmass is MS mass subtracted and calculated LPL average mass $(M + H)^+$ assuming 1,039 Da per N-linked glycosylation site for human and mLPL expressed in S2 cells.

Protein stability

Protein stability was analyzed by thermal unfolding experiments with nanodifferential scanning fluorimetry using a Prometheus NT.48™ (Nanotemper) to record changes in intrinsic tryptophan or tyrosine fluorescence (excitation of 280 nm and emission of 330 and 350 nm) (38). Thermal unfolding of LPL and GPIHPB1 complexes was determined for 5 μM LPL and 5 μM GPIHBP1 in 10 mM Tris-HCl (pH 7.2) and increasing NaCl concentrations (0.2, 0.4, 0.8, and 1.2 M NaCl) and at 1.2 M NaCl, 40% glycerol, and 10 mM Tris-HCl (pH 7.2). The complexes were preincubated for 2 min at 4°C to allow complex formation, cleared by centrifugation at 20,000 g for 10 min (4°C), and then loaded into capillaries. For determination of thermal unfolding of LPL at the different salt and glycerol concentrations, 10 μM LPL was used. A linear temperature ramp of 1°C per minute from 20 to 90°C was used to unfold the samples. The first derivative of the fluorescence ratio between 350/330 nm was used to determine melting temperature (T_m).

RESULTS

Coexpression of LPL with LMF1 and GPIHBP1 in *Drosophila* S2 cells

The primary objective of this study was to develop an efficient and robust protocol for the expression and purification of recombinant hLPL that could supply large quantities of high-quality LPL in a pure and stable form and with high specific enzymatic activity. Since previous protocols for LPL production often used the LPL[R297A] mutation to avoid undesirable furin cleavages during production (18, 39), we initially included this mutation in the optimization of our LPL expression system (Fig. 1). Building on our previous biophysical data showing that bLPL has a T_m of only 34.8°C (23), we chose *Drosophila* S2 cells as the heterologous host cells for hLPL expression because these cells grow efficiently at 25°C compared with the 37°C required for most mammalian expression systems. To establish the impact of known stabilizing proteins (LMF1 and GPIHBP1) on the expression yields and quality of recombinant hLPL, we produced four different *Drosophila* S2 cell lines expressing hLPL[R297A] in the absence or the presence of membrane-bound hLMF1 and soluble hGPIHBP1. Notably, these experiments revealed a clear and differential progression in the average yields of purified LPL (Table 1). We thus obtained 0.3 mg/l cultured medium for hLPL[R297A] alone, 0.7 mg/l cultured medium for hLPL[R297A] coexpressed with hGPIHBP1, 2.2 mg/l cultured medium for hLPL[R297A] coexpressed with hLMF1, whereas a synergistic effect was obtained for hLPL[R297A] coexpressed with both hLMF1 and hGPIHBP1 (13.5 mg/l cultured medium). These yields are consistent with a biosynthetic pathway in transfected S2 cells where LPL first encounters the chaperone LMF1 in the endoplasmic reticulum facilitating its correct folding and subsequently encounters GPIHBP1 that acts to stabilize LPL both in the downstream secretory pathway and in the culture media. This sequential chaperoning of LPL is nicely recapitulated by the observations that coexpression with hGPIHBP1 produces low amounts of purified LPL with high specific activity, whereas coexpression with only hLMF1 produces higher amounts of LPL, but with lower specific activity (Table 1). We employed a one-step purification of hLPL from the CM using a 1 ml HiTrap™ heparin-Sepharose column controlled by an Äkta Purifier™ (GE Healthcare). After extensive washing with ~25 ml buffer consisting of 0.9 M NaCl, 10 mM Bis-Tris (pH 6.5), and 10% glycerol, the bound LPL was eluted with a 12 ml linear gradient from 0.9 to 2 M NaCl, and the elution of hLPL peaked at a conductivity of 78 mS/cm corresponding to 1.3 M NaCl (**Fig. 2**A). The eluted fractions were analyzed with SDS-PAGE, and the Coomassie-stained polyacrylamide gels revealed a remarkably pure LPL preparation without detectable GPIHBP1 and with only a very few and low abundant protein contamination (Fig. 2B). An optional concentration and buffer exchange of the collected LPL fractions could conveniently be accomplished by a subsequent
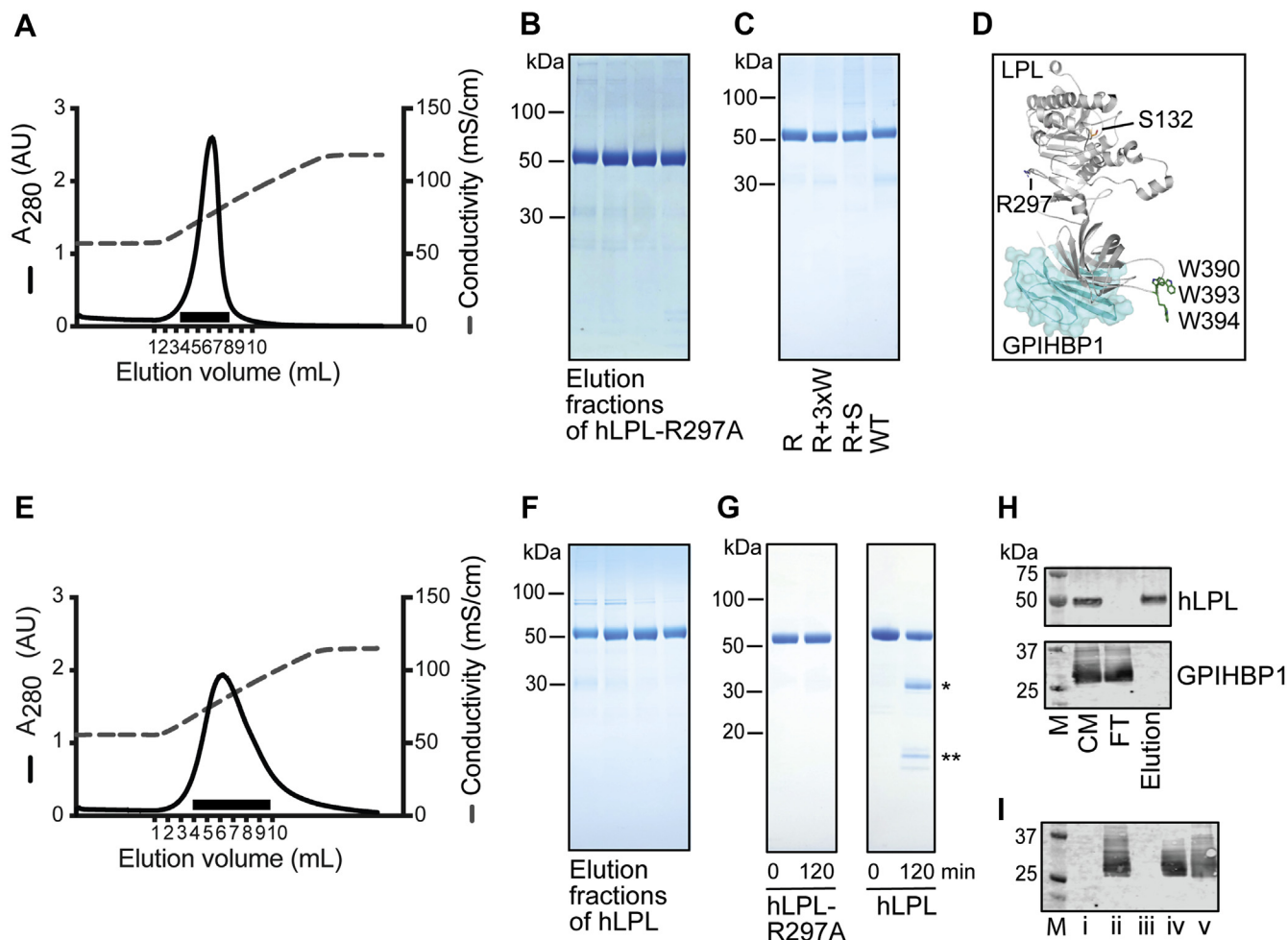
Fig. 2. Single-step purification of hLPL. A: The elution profile from HiTrap™ heparin column is shown for hLPL^{R297A} coexpressed with hLMF1 and hGPIHBP1. The black line shows UV absorbance at 280 nm (AU), and the dashed line shows the increasing conductivity during the NaCl-gradient elution. B: SDS-PAGE of the collected hLPL^{R297A} fractions from the HiTrap™ heparin column (indicated with a black bar in A). C: SDS-PAGE gel of the ammonium sulphate-precipitated samples for hLPL^{R297A} (R), hLPL$^{R297A-W390A-W393A-W394A}$ (3xW), hLPL$^{S132A-R297A}$ (R + S), and hLPL (wt). D: The structure of hLPL with indication of the R297A mutation, the loop containing the W390A-W393A-W394A mutations, and the active site with the S132A mutation. E: The elution profile from HiTrap™ heparin column for hLPL coexpressed with hLMF1 and hGPIHBP1 represented as in (A). F: SDS-PAGE of the collected hLPL fractions from the HiTrap™ heparin column (indicated with a black bar in E). G: Purified hLPL^{R297A} and hLPL incubated with furin for 0 and 120 min. The N-terminal fragment of hLPL is marked with *, and the C-terminal fragment of hLPL is marked with **. H: Western blot of a purification of hLPL assessing the presence of hLPL and hGPIHBP1 in *i*) the CM, *ii*) flow through (FT), and *iii*) the peak elution fraction after applying the NaCl gradient. The molecular weight marker is in lane M. I: Assessing the expression of hGPIHPB1 with Western blot of CM from cells transfected with *i*) hLPL^{R297A}; *ii*) hLPL^{R297A} and hGPIHBP1; *iii*) hLPL^{R297A} and hLMF1; *iv*) hLPL^{R297A}, hGPIHBP1, and hLMF1; and *v*) hLPL, hGPIHBP1, and hLMF1.

precipitation step by dialysis into 3.6 M (NH$_4$)$_2$SO$_4$ and 50 mM Bis-Tris (pH 6.5) at 4°C (Fig. 2C). This procedure furthermore eliminated the majority of the trace impurities found in the eluates from the heparin-Sepharose column yielding a very pure and concentrated LPL preparation (Fig. 2C).

We were curious to challenge the robustness and versatility of this protocol for LPL production, and we therefore tested its performance with different LPL mutants. The lipase-inactive variants, hLPL$^{R297A-W390A-W393A-W394A}$ and hLPL$^{S132A-R297A}$ (Fig. 2D), were coexpressed with hLMF1 and hGPIHBP1 and purified using our new protocol. Both LPL mutants expressed well and yielded very pure preparations with average

yields of 3.7–4.7 mg/l, respectively (Table 1 and Fig. 2C). Finally, we argued that the coexpression of LPL with GPIHBP1 would minimize the risk for furin cleavage at R297 during expression, since we previously showed that GPIHBP1 efficiently protected LPL from furin cleavage using purified proteins (28). We therefore repeated our expression protocol with wt hLPL devoid of any mutations. This procedure provided a remarkably high yield of pure hLPL with an average of 28.2 mg purified hLPL per liter of CM (Fig. 2E, F). The purified hLPL is sensitive to furin cleavage in vitro, whereas purified hLPL^{R297A} is resilient to cleavage. This is clearly observed by the formation of an N-terminal (N-terminal domain$^{1–312}$) and
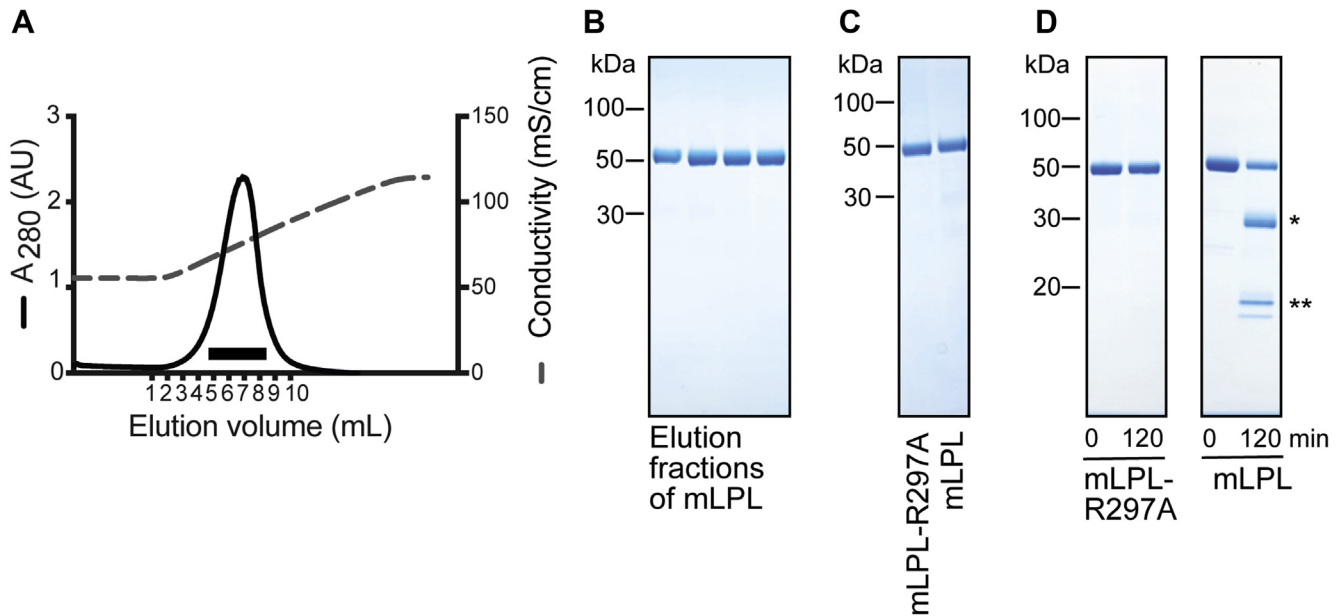
Fig. 3. Single-step purification of mLPL. A: The elution profile from HiTrap™ heparin column is shown for mLPL coexpressed with mLMF1 and mGPIHBP1. The black line shows UV absorbance at 280 nm (mAU), and the dashed line shows the increasing conductivity during the NaCl-gradient elution of mLPL. B: SDS-PAGE of the collected mLPL fractions from the HiTrap™ heparin column (as indicated with a black bar in A). C: SDS-PAGE gel of the ammonium sulphate-precipitated samples for mLPL[R297A] and mLPL. D: mLPL[R297A] and mLPL incubated with furin for 0 and 120 min. The N-terminal fragment of mLPL is marked with *, and the C-terminal fragment of mLPL is marked with **.

C-terminal (C-terminal domain[313–448]) LPL fragment after incubation of wt LPL in the presence of furin for 2 h at 25°C (Fig. 2G)—replicating previous findings for endogenous bLPL purified from cow milk (28). The intact mass of the different LPL variants was determined with MALDI-TOF MS, and only slight variation was observed, as compared with the calculated average mass with both N-linked glycosylation site occupied, indicating purification of intact glycosylated LPL (Table 1).

It was clear that coexpression with hLMF1 and hGPIHBP1 greatly increased the yields of hLPL. To confirm that hGPIHBP1 was indeed coexpressed with LPL and eluted in the flow through of the heparin-Sepharose chromatography, we performed Western blot analysis with the monoclonal antibodies 5D2 recognizing hLPL (29) and R2 targeting the suPAR-DIII tag in the GPIHBP1 construct (31). This verified the presence of both hLPL and hGPIHBP1 in the CM and demonstrated that only LPL was bound to and eluted from the heparin-Sepharose column, whereas GPIHBP1 appeared in the flow through during application of the CM (Fig. 2H). Expression of hGPIHBP1 was also confirmed in the CM from the stable transfections of hLPL[R297A] + hGPIHBP1, hLPL[R297A] + hGPIHBP1 + hLMF1, and hLPL + hGPIHBP1 + hLMF1 (Fig. 2I). Optionally, GPIHBP1 can be purified from the run-through of the heparin-Sepharose chromatography with affinity chromatography utilizing either the affinity tag or a monoclonal anti-GPIHBP1 antibody (not shown).

We next assessed the specific enzymatic activity of the purified LPL preparations. Measuring the lipase activity with long-chain triacylglycerol emulsions as substrate and quantifying the release of NEFA assay analysis revealed that hLPL and hLPL[R297A] preparations had the same high specific activity, whereas preparations of hLPL[R297A-W390A-W393A-W394A] and hLPL[S132A-R297A] as expected were devoid of lipase activity (Table 1). When assessing the hydrolytic activity toward a short-chain soluble synthetic substrate (DGGR), we found that hLPL and hLPL[R297A] again had similar esterase activities, hLPL[R297A-W390A-W393A-W394A] had lower but discernible esterase activity, whereas hLPL[S132A-R297A] was inactive, as was predicted from its compromised catalytic triad.

Expression and purification of mLPL

As a final challenge of the versatility of our expression and purification protocol, we explored its potential to express and purify LPL from a different species. We accordingly established *Drosophila* S2 cells that were cotransfected with mLPL[R297A] (or mLPL), mLMF1, and mGPIHBP1. From these culture supernatants, we purified 7.4 and 8.4 mg/l enzymatic active mLPL[R297A] and mLPL, respectively (Table 1). The elution fractions contained highly pure mLPL as assessed by Coomassie-stained polyacrylamide gels after SDS-PAGE (Fig. 3A–C). The specific lipase and esterase activities of mLPL (Table 1), differential sensitivity toward furin cleavage between mLPL[R297A] and mLPL (Fig. 3D), and differential thermostability between mLPL and

LPL variants	k_{on} (10^6 M^{-1} s^{-1})	k_{off} (10^{-3} s^{-1})	K_D (nM)	LPL[b] T_m (°C)	LPL·GPIHBP1[b] T_m (°C)
hLPL-R297A	3.20 ± 0.07	2.18 ± 0.02	0.68	30.5 ± 0.9	55.2 ± 0.6
hPL-S132A-R297A	2.41 ± 0.12	2.51 ± 0.06	1.05	31.5 ± 0.4	56.6 ± 0.3
hLPL-R297A-W390A-W393A-W394A	NA[a]	NA[a]	NA[a]	28.4 ± 0.2	NA[d]
hLPL	3.87 ± 0.02	2.76 ± 0.04	0.71	36.6 ± 0.2	57.3 ± 0.7
mLPL-R297A	NA[a]	NA[a]	NA[a]	28.9 ± 0.1	49.7 ± 0.8
mLPL	NA[a]	NA[a]	NA[a]	29.1 ± 0.2	51.0 ± 0.6
bLPL	3.40 ± 0.11	5.20 ± 0.08	1.54	34.8 ± 0.1[c]	57.6 ± 0.1[c]

NA, not available.
The ligand used for the various interactions with the different LPL variants is in all cases hGPIHBP1[1–131] (27).
[a]The kinetic rate constant for these proteins could not be determined since 5D2 is unable to capture these molecules (37, 40).
[b]The apparent T_m for LPL incubated alone or in the presence of GPIHBP1 at 0.2 M NaCl, pH 7.2 was measured by the first derivative of the ratio between 350/330 nm. All profiles were measured in triplicates with mean T_m and standard derivation reported.
[c]These values were determined in another study (23) with proteins mixed in 0.15 M NaCl and 10 mM Hepes (pH 7.4).
[d]The PR.ThermControl analysis software were unable to automatically assign T_m for N-terminal domain of LPL.

mLPL·hGPIHBP1 complexes (Table 2) recapitulate the properties we measured for purified hLPL.

Biochemical characterization of the purified recombinant hLPL preparations

In addition to lipase and esterase activity measurements (Table 1), we determine the real-time binding kinetics between the purified hLPL variants and a soluble form of hGPIHBP1 using SPR as outlined previously for studies on bLPL (27, 36). The quality of the SPR analyses critically depends on presenting a uniformly orientated and relatively stable LPL on the biosensor surface. We accomplished that by using a covalently immobilized monoclonal anti-LPL antibody (5D2) as capturing principle for the unmodified purified LPL. As shown in **Fig. 4**A and Table 2, we found comparable kinetic rate constants for hGPIHBP1 binding to hLPL, hLPL[R297A], and hLPL[S132A-R297A], and the real-time binding kinetics are characterized by relatively fast on-rates (k_{on}) and equilibrium dissociation constants (K_D) in the lower nanomolar range. For comparison, we also determined the rate constants for bLPL binding to hGPIHBP1 in a parallel single-cycle analysis. Unfortunately, this protocol precludes measurements with mLPL that does not bind 5D2, and the hLPL[R297A-W390A-W393A-W394A] variant as the mutations in the Trp-rich lipid-binding loop disrupts the epitope on LPL for 5D2 (37, 40). The ability of GPIHBP1 to bind purified hLPL[R297A-W390A-W393A-W394A] and mLPL samples was therefore verified and compared with hLPL by native polyacrylamide gel analysis. Because of its high isoelectric point, hLPL migrates slowly and appears as a smear in native PAGE, whereas GPIHBP1 (low isoelectric point) and GPIHBP1·LPL complexes migrate faster and as well-defined bands (Fig. 4B). This clearly shows that both mLPL and hLPL[R297A-W390A-W393A-W394A] bind hGPIHBP1. Preincubation of hLPL·hGPIHBP1 complex in the presence of intralipid emulsions prevented migration of the complex during native PAGE because of the lipid-binding properties of the tryptophan-rich loop. Decoupling the lipid binding of the tryptophan-rich loop by alanine replacement rendered the electrophoretic migration of the hLPL[R297A-390A-W393A-W394A]·hGPIHBP1 complexes largely insensitive to the presence of lipid emulsions (Fig. 4C).

Finally, we determined the thermal stability of the different purified hLPL variants with differential scanning fluorimetry. We found that the N-terminal α/β-hydrolase domain in hLPL[R297A] exhibits low thermal stability with a T_m of 30.5°C, and this undergoes a dramatic increase to T_m of 55.2°C after binding to GPIHBP1 (Table 2 and Fig. 4D). This stability profile largely recapitulates that found previously for endogenous bLPL purified from cow milk (23). The analysis software were not able to automatically assign T_m for N-terminal domain of hLPL[R297A-W390A-W393A-W394A], but the back-reflection reporting protein aggregation showed that $T_{turbidity}$ for LPL was shifted from 29.5 ± 0.4°C in the absence of GPIHBP1 to 59.2 ± 0.1°C in the presence of GPIHBP1. The thermal stabilities of hLPL, hLPL[S132A-R297A], mLPL, and mLPL[R297A] were comparable to hLPL[R297A], and all experienced a pronounced stabilization by GPIHBP1 binding (Table 2 and Fig. 4D, E).

Formulation of purified LPL to bolster long-term stability

To optimize long-term stability of our purified LPL preparations, we initially measured thermal stability of hLPL and mLPL preparations at increasing ion strengths: 0.2, 0.4, 0.8, and 1.2 M NaCl in 10 mM Tris-HCl (pH 7.2). These studies revealed a progressive increase in hLPL[R297A] thermostability from T_m = 30.5°C (0.2 M NaCl) to T_m = 39.5°C (1.2 M NaCl) (Table 3 and **Fig. 5**A). The thermostability of purified hLPL, mLPL[R297A], and mLPL showed a similar dependency of the ion strength of the storage buffer (Table 3 and Fig. 5A, B). We went on to test the stabilizing effect of glycerol—a commonly used excipient added to stabilize purified LPL preparations. As shown in Table 3, the addition of 0–40% (v/v)
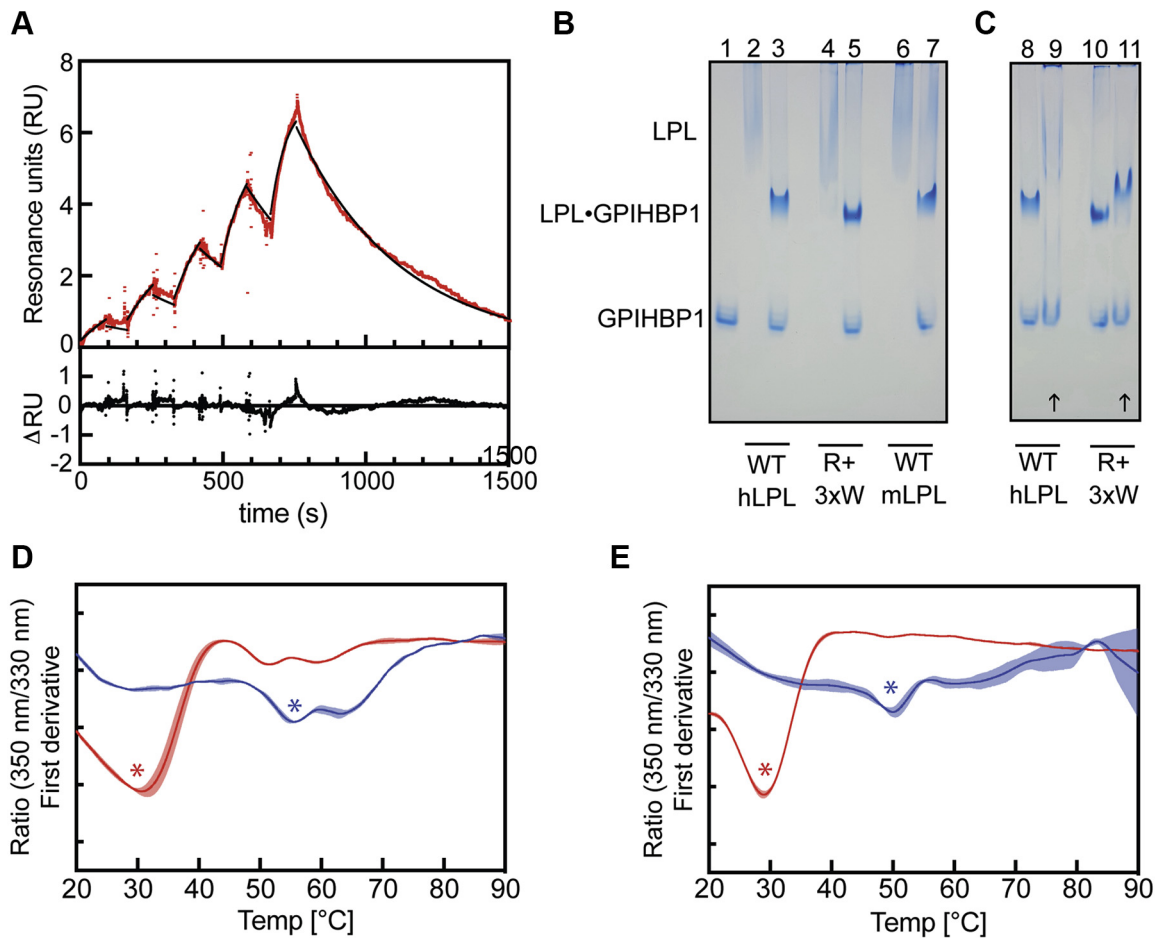
Fig. 4. Verification of LPL·GPIHBP1 interactions with SPR, native PAGE, and nanodifferential scanning fluorimetry. A: Determination of the real-time kinetics of the hLPL·hGPIHBP1 interaction by single-cycle SPR. LPL was captured on a CM4 sensor chip by an immobilized anti-LPL monoclonal antibody (5D2). The figure shows the buffer-referenced sensorgram (in red) recorded for sequential injections of 0.5, 1, 2, 4, and 8 nM hGPIHBP1. Mathematical fitting to a simple 1:1 binding model is superimposed as black lines on the sensorgram. Residuals from the fit are shown. B: Pairwise native PAGE analysis of LPL and LPL·GPIHBP1 complexes: hLPL (lanes 2 and 3); hLPL[R297A-W390A-W393A-W394A] (lanes 4 and 5); and mLPL (lanes 6 and 7). Lane 1 is GPIHBP1. C: Native PAGE analysis of LPL·GPIHBP1 complexes in the absence (lanes 8 and 10) or the presence of intralipid emulsion in the application wells (lanes 9 and 11): hLPL (lanes 8 and 9) and hLPL[R297A-W390A-W393A-W394A] (lanes 10 and 11). D: First derivative of the thermal unfolding profiles plotted as the ratio between 350 and 330 nm of hLPL[R297A] in the absence (red line) and the presence of hGPIHBP1 (blue line) at 0.2 M NaCl (pH 7.2). E: Thermal unfolding profiles of mLPL[R297A] in the absence (red line) and presence of hGPIHBP1 (blue line). Shown is the mean of the first derivative of the ratio of emission intensity at 350 and 330 nm wavelength as a function of increasing temperature with standard derivation indicated in transparent colors. The apparent T_m for the N-terminal α/β-hydrolase domain (NTD[1-312]) of LPL is highlighted with a colored asterisk.

glycerol to hLPL[R297A] progressively increased the thermostability by ∼11°C in the presence of 0.2 M NaCl (T_m = 30.5 to T_m = 41.3°C). Glycerol also had an advantageous effect on the thermostability of hLPL[R297A] in the presence of 1.2 M NaCl (T_m = 39.5°C without glycerol and T_m = 42.9°C in the presence of 40% [v/v] glycerol). The thermostability of purified hLPL, mLPL[R297A], and mLPL showed a similar increase in the presence of these excipients (Table 3 and Fig. 5A, B).

Having delineated the advantageous effect of high ion strengths and glycerol on thermostability, we tested the time-dependent perseverance of the enzymatic activity of LPLs at different temperatures (from −80 to 23°C) in buffers containing *i*) 0.2 M NaCl, *ii*) 0.2 M NaCl with 40% (v/v) glycerol, and *iii*) 1.2 M NaCl with 40% (v/v) glycerol in 10 mM Tris-HCl, pH 7.2 (Fig. 5C–F). In

these stability studies, we subjected 1 mg/ml of hLPL[R297A] to the given incubation conditions, and after a 3000-fold dilution of LPL, we followed the specific lipase activity with NEFA activity measurements on withdrawn aliquots. When hLPL[R297A] was stored in 0.2 M NaCl at 23°C, the specific activity declined rapidly and was undetectable after 8 h at 23°C (Fig. 5C). Adding 40% glycerol to the buffer with 0.2 M NaCl increased the perseverance of the lipase activity of LPLs at both 4 and 23°C, and only a negligible decline occurred upon incubation at 4°C for 10 days (Fig. 5C, D). Short-term storage for up to 21 days at −20°C or −80°C did not lead to any detectable loss of activity in either of the storage buffers. A few repeated cycles of freeze and thaw did not cause detectable loss in lipase activity (Fig. 5E, F).

TABLE 3. Thermal stability of LPL at increasing NaCl and glycerol concentrations

Sample condition[a]	hLPL-R297A	hLPL	mLPL-R297A	mLPL
	T_m (°C)			
0.2 M NaCl	30.5 ± 0.9	36.6 ± 0.2	28.9 ± 0.1	29.1 ± 0.2
0.4 M NaCl	32.9 ± 0.3	37.1 ± 0.6	31.3 ± 0.2	31.5 ± 0.5
0.8 M NaCl	36.8 ± 0.1	37.9 ± 0.2	34.5 ± 0.1	34.7 ± 0.1
1.2 M NaCl	39.5 ± 0.1	40.5 ± 0.1	36.7 ± 0.1	37.4 ± 0.3
0.2 M NaCl, 10% glycerol	34.4 ± 0.1	39.1 ± 0.1	33.4 ± 0.3	34.8 ± 0.4
0.2 M NaCl, 20% glycerol	38.0 ± 0.1	44.0 ± 0.3	36.7 ± 0.2	39.7 ± 0.5
0.2 M NaCl, 40% glycerol	41.3 ± 0.5	45.5 ± 0.2	41.5 ± 0.1	46.6 ± 0.2
1.2 M NaCl, 40% glycerol	42.9 ± 0.0	46.6 ± 0.3	42.7 ± 0.1	46.4 ± 0.4

[a]The apparent T_m was measured for the indicated sample conditions at pH 7.2 by changes in endogenous tryptophan fluorescence (measured as the 350/330 nm ratio). The mean and standard derivations for T_m are shown (n = 3).

DISCUSSION

The first atomic structure of LPL determined by X-ray crystallography was reported in 2019 (19)—more than seven decades after its discovery (41). The extraordinary long delay before obtaining this important structural information was not because of a lack of biological or medical significance, as an early study thus reported LPL as the first example of an inborn error in plasma lipid metabolism (42). Major roadblocks to the progress in solving the crystal structure of hLPL were the inherent protein instability and aggregation-prone nature of purified LPL paired with the lack of a suitable expression system yielding large quantities of monodisperse protein. The discovery of GPIHBP1 being an endothelial-binding partner for LPL (43) and that its binding to LPL prevents the spontaneous unfolding of the α/β-hydrolase domain of LPL (27) was instrumental for solving the atomic structure of LPL (19). Notwithstanding this achievement, the post-crystallographic era in LPL research still calls for new and efficient protocols to produce high-quality recombinant hLPL and disease-relevant mutants of LPL. Future studies on hLPL conformation and dynamics using hydrogen-deuterium exchange MS (27, 44), small-angle X-ray scattering (40), cryogenic electron microscopy (45), nanodifferential scanning fluorimetry (23), and SPR (36) are all dependent on a reliable source of recombinant LPL production. Such studies would ideally provide a wealth of essential information on *i*) the protein stability of biological relevant LPL variants, *ii*) the binding site(s) for various LPL ligands, and *iii*) the allosteric landscape of LPL as a function of ligand binding.

In the present study, we developed such a generally accessible and robust expression and purification platform for recombinant LPL production. Building on previous knowledge on purified bLPL stability and biosynthesis of hLPL (23, 24, 26), we sought to optimize LPL stability in all compartments during its biosynthesis and secretion. The hallmarks of this protocol are *i*) the use of *Drosophila* S2 cells as heterologous expression host, which can grow in suspension at low temperature (25°C) and at high cell density, *ii*) coexpression of the chaperone LMF1, *iii*) coexpression of GPIHBP1 to substitute for syndecan-1 in the *trans*-Golgi secretory pathway, to stabilize the secreted LPL in the conditioned cell culture medium during the induction time, and to prevent its association to cell surfaces, and *iv*) the implementation of heparin-Sepharose affinity chromatography that serves a dual purpose: it provides a convenient and high-capacity one-step purification of LPL (33) combined with its ability to disrupt the LPL·GPIHBP1 complexes during application of the CM (Figs. 2 and 3). During sample application, LPL is stabilized by the immobilized heparin and low temperature (46), whereas the high ion strength provides stabilization of LPL during elution (Table 3 and Fig. 5). Using differential scanning fluorimetry and activity assays, we found that a 10 mM Tris-HCl buffer (pH 7.2) with 1.2 M NaCl and 40% (v/v) glycerol was ideal for storage of ≥1 mg/ml stock solutions of purified hLPL (Fig. 5).

We predict that this protocol will be useful for future studies on LPL biology and biochemistry and provide high-quality LPL variants with defined mutations for structure-function studies. In the present study, we have used a polyclonal S2 cell line for LPL production and limited the production scheme to include only three consecutive harvests of CM to avoid decline in LPL secretion. It is however very likely that the yields of LPL can be optimized further by establishing a true monoclonal cell line that robustly produces higher levels of LPL during multiple rounds of serial harvests without loss of expression (47). Such considerations are particular relevant when a given LPL variant is needed in very high quantities, for example, in large-scale drug screening programs. Our observation that two parallel transfections with the same constructs could result in quite different average yields for hLPL (28.2 vs. 6.0 mg/ml) put further emphasis on the virtues of using monoclonal cell lines for future large-scale productions. We observed a lower specific activity for our recombinant hLPL preparations compared with bLPL purified from milk (Table 1). Whether this difference relates to inherent species-specific differences in the LPL activity between man and cattle or is caused by the lower complexity in the glycans attached by *Drosophila* S2 cells remains to be clarified. Although the glycans produced by *Drosophila* S2 cells differ from those produced by mammalian host cells (32), this expression system may also be useful for the initial attempts at producing LPL variants with increased thermostability and lower sensitivity to endogenous LPL inhibitors like angiopoietin-like proteins 3, 4, and 8. If successful, such variants expressed in a suitable host could be useful for
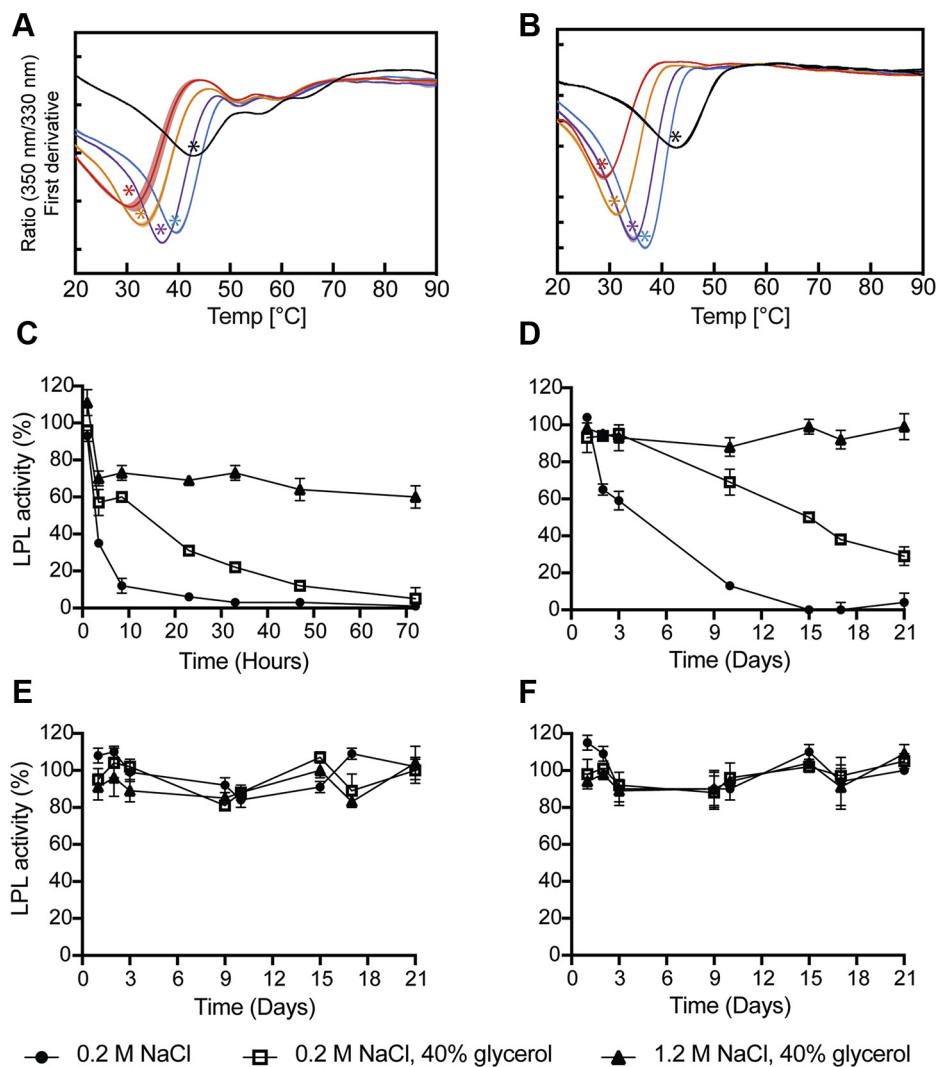
Fig. 5. Thermal and shelf-life stability of hLPL at different conditions. A: Thermal unfolding profiles of hLPL^{R297A} in the presence of 0.2 M NaCl (red line), 0.4 M NaCl (orange line), 0.8 M NaCl (purple line), 1.2 M NaCl (blue line), 1.2 M NaCl, and 40% glycerol in 10 mM Tris-HCl (pH 7.2) (black line). Shown are the means of the first derivative of the ratio of emission intensity at 350 and 330 nm wavelength as a function of increasing temperature with standard derivation indicated in transparent colors. The apparent T_m for the N-terminal α/β-hydrolase domain (NTD$^{1-312}$) of LPL is highlighted with a colored asterisk. The C-terminal lipid-binding domain of hLPL (CTD$^{313-448}$) has a T_m of 58.7 ± 0.3°C determined in another study (23). B: The corresponding unfolding profiles are shown for mLPL^{R297A}. C: hLPL^{R297} was stored at 1 mg/ml at 0.2 M NaCl, pH 7.2 (closed circles), 0.2 M NaCl, 40% glycerol, pH 7.2 (open squares), and 1.2 M NaCl, 40% glycerol, pH 7.2 (closed triangles) at 23°C, (D) 4°C, (E) −20°C, and (F) −80°C. The LPL activity was measured at the indicated time points and normalized to average LPL activity for the first time point at each temperature tested.

enzyme replacement therapy in patients with monogenic familiar LPL deficiency.

Data availability

All data are contained within the article.

Author ORCIDs

Anne-Marie Lund Winther https://orcid.org/0000-0002-5776-0989

Kristian Kølby Kristensen https://orcid.org/0000-0003-3190-5411

Anni Kumari https://orcid.org/0000-0001-8245-269X

Michael Ploug https://orcid.org/0000-0003-2215-4265

REFERENCES

1. Young, S. G., Fong, L. G., Beigneux, A. P., Allan, C. M., He, C., Jiang, H., Nakajima, K., Meiyappan, M., Birrane, G., and Ploug, M. (2019) GPIHBP1 and lipoprotein lipase, partners in plasma triglyceride metabolism. *Cell Metab.* **30**, 51–65
2. Davies, B. S., Beigneux, A. P., Barnes, R. H., Tu, Y., Gin, P., Weinstein, M. M., Nobumori, C., Nyrén, R., Goldberg, I., Olivecrona, G., Reue, K., Tontonoz, P., Bensadoun, A., Beigneux, A. P., Young, S. G., *et al.* (2010) GPIHBP1 is responsible for the entry of lipoprotein lipase into capillaries. *Cell Metab.* **12**, 42–52
3. Goulbourne, C. N., Gin, P., Tatar, A., Nobumori, C., Hoenger, A., Jiang, H., Grovenor, C. R., Adeyo, O., Esko, J. D., Goldberg, I. J., Reue, K., Tontonoz, P., Bensadoun, A., Beigneux, A. P., Young, S. G., *et al.* (2014) The GPIHBP1-LPL complex is responsible for the margination of triglyceride-rich lipoproteins in capillaries. *Cell Metab.* **19**, 849–860
4. Dron, J. S., and Hegele, R. A. (2020) Genetics of hypertriglyceridemia. *Front. Endocrinol. (Lausanne).* **11**, 455
5. Beigneux, A. P., Miyashita, K., Ploug, M., Blom, D. J., Ai, M., Linton, M. F., Khovidhunkit, W., Dufour, R., Garg, A., McMahon, M. A., Pullinger, C. R., Sandoval, N. P., Hu, X., Allan, C. M., Larsson, M., *et al.* (2017) Autoantibodies against GPIHBP1 as a cause of hypertriglyceridemia. *N. Engl. J. Med.* **376**, 1647–1658
6. Warden, B. A., and Duell, P. B. (2021) Evinacumab for treatment of familial hypercholesterolemia. *Expert Rev. Cardiovasc. Ther.* **19**, 739–751
7. Ng, D. S. (2021) Evolving ANGPTL-based lipid-lowering strategies and beyond. *Curr. Opin. Lipidol.* **32**, 271–272
8. Fowler, A., Sampson, M., Remaley, A. T., and Chackerian, B. (2021) A VLP-based vaccine targeting ANGPTL3 lowers plasma triglycerides in mice. *Vaccine.* **39**, 5780–5786
9. Hegele, R. A., Berberich, A. J., Ban, M. R., Wang, J., Digenio, A., Alexander, V. J., D'Erasmo, L., Arca, M., Jones, A., Bruckert, E., Stroes, E. S., Bergeron, J., Civeira, F., Witztum, J. L., Gaudet, D., *et al.* (2018) Clinical and biochemical features of different molecular etiologies of familial chylomicronemia. *J. Clin. Lipidol.* **12**, 920–927.e4
10. Scott, L. J. (2015) Alipogene tiparvovec: A review of its use in adults with familial lipoprotein lipase deficiency. *Drugs.* **75**, 175–182
11. Bengtsson-Olivecrona, G., and Olivecrona, T. (1991) Phospholipase activity of milk lipoprotein lipase. *Methods Enzymol.* **197**, 345–356
12. Hayashi, R., Tajima, S., and Yamamoto, A. (1986) Purification and characterization of lipoprotein lipase from human postheparin plasma and its comparison with purified bovine milk lipoprotein lipase. *J. Biochem.* **100**, 319–331
13. Chen, Y. Q., Pottanat, T. G., Siegel, R. W., Ehsani, M., Qian, Y. W., Zhen, E. Y., Regmi, A., Roell, W. C., Guo, H., Luo, M. J., Gimeno, R. E., Van't Hooft, F., and Konrad, R. J. (2020) Angiopoietin-like protein 8 differentially regulates ANGPTL3 and ANGPTL4 during postprandial partitioning of fatty acids. *J. Lipid Res.* **61**, 1203–1220
14. Chi, X., Britt, E. C., Shows, H. W., Hjelmaas, A. J., Shetty, S. K., Cushing, E. M., Li, W., Dou, A., Zhang, R., and Davies, B. S. J. (2017) ANGPTL8 promotes the ability of ANGPTL3 to bind and inhibit lipoprotein lipase. *Mol. Metab.* **6**, 1137–1149
15. Beigneux, A. P., Fong, L. G., Bensadoun, A., Davies, B. S., Oberer, M., Gårdsvoll, H., Ploug, M., and Young, S. G. (2015) GPIHBP1 missense mutations often cause multimerization of GPIHBP1 and thereby prevent lipoprotein lipase binding. *Circ. Res.* **116**, 624–632
16. Voss, C. V., Davies, B. S., Tat, S., Gin, P., Fong, L. G., Pelletier, C., Mottler, C. D., Bensadoun, A., Beigneux, A. P., and Young, S. G. (2011) Mutations in lipoprotein lipase that block binding to the endothelial cell transporter GPIHBP1. *Proc. Natl. Acad. Sci. U.S.A.* **108**, 7980–7984
17. Beigneux, A. P., Allan, C. M., Sandoval, N. P., Cho, G. W., Heizer, P. J., Jung, R. S., Stanhope, K. L., Havel, P. J., Birrane, G., Meiyappan, M., Gill, J. E., Murakami, M., Miyashita, K., Nakajima, K., Ploug, M., *et al.* (2019) Lipoprotein lipase is active as a monomer. *Proc. Natl. Acad. Sci. U.S.A.* **116**, 6319–6328
18. Wu, M. J., Wolska, A., Roberts, B. S., Pearson, E. M., Gutgsell, A. R., Remaley, A. T., and Neher, S. B. (2018) Coexpression of novel furin-resistant LPL variants with lipase maturation factor 1 enhances LPL secretion and activity. *J. Lipid Res.* **59**, 2456–2465
19. Birrane, G., Beigneux, A. P., Dwyer, B., Strack-Logue, B., Kristensen, K. K., Francone, O. L., Fong, L. G., Mertens, H. D. T., Pan, C. Q., Ploug, M., Young, S. G., and Meiyappan, M. (2019) Structure of the lipoprotein lipase–GPIHBP1 complex that mediates plasma triglyceride hydrolysis. *Proc. Natl. Acad. Sci. U.S.A.* **116**, 1723–1732
20. Arora, R., Nimonkar, A. V., Baird, D., Wang, C., Chiu, C. H., Horton, P. A., Hanrahan, S., Cubbon, R., Weldon, S., Tschantz, W. R., *et al.* (2019) Structure of lipoprotein lipase in complex with GPIHBP1. *Proc. Natl. Acad. Sci. U.S.A.* **116**, 10360–10365
21. Nimonkar, A. V., Weldon, S., Godbout, K., Panza, D., Hanrahan, S., Cubbon, R., Xu, F., Trauger, J. W., Gao, J., and Voznesensky, A. (2020) A lipoprotein lipase-GPI-anchored high-density lipoprotein-binding protein 1 fusion lowers triglycerides in mice: Implications for managing familial chylomicronemia syndrome. *J. Biol. Chem.* **295**, 2900–2912
22. Kristensen, K. K., Leth-Espensen, K. Z., Kumari, A., Grønnemose, A. L., Lund-Winther, A. M., Young, S. G., and Ploug, M. (2021) GPIHBP1 and ANGPTL4 utilize protein disorder to orchestrate order in plasma triglyceride metabolism and regulate compartmentalization of LPL activity. *Front. Cell Dev. Biol.* **9**, 702508
23. Leth-Espensen, K. Z., Kristensen, K. K., Kumari, A., Winther, A. L., Young, S. G., Jørgensen, T. J. D., and Ploug, M. (2021) The intrinsic instability of the hydrolase domain of lipoprotein lipase facilitates its inactivation by ANGPTL4-catalyzed unfolding. *Proc. Natl. Acad. Sci. U.S.A.* **118**, e2026650118
24. Sundberg, E. L., Deng, Y., and Burd, C. G. (2019) Syndecan-1 mediates sorting of soluble lipoprotein lipase with sphingomyelin-rich membrane in the golgi apparatus. *Dev. Cell.* **51**, 387–398.e4
25. Koerner, C. M., Roberts, B. S., and Neher, S. B. (2019) Endoplasmic reticulum quality control in lipoprotein metabolism. *Mol. Cell. Endocrinol.* **498**, 110547
26. Péterfy, M., Ben-Zeev, O., Mao, H. Z., Weissglas-Volkov, D., Aouizerat, B. E., Pullinger, C. R., Frost, P. H., Kane, J. P., Malloy, M. J., Reue, K., Pajukanta, P., and Doolittle, M. H. (2007) Mutations in LMF1 cause combined lipase deficiency and severe hypertriglyceridemia. *Nat. Genet.* **39**, 1483–1487
27. Mysling, S., Kristensen, K. K., Larsson, M., Beigneux, A. P., Gårdsvoll, H., Fong, L. G., Bensadouen, A., Jørgensen, T. J., Young, S. G., and Ploug, M. (2016) The acidic domain of the endothelial membrane protein GPIHBP1 stabilizes lipoprotein lipase activity by preventing unfolding of its catalytic domain. *Elife.* **5**, e12095
28. Lund Winther, A. M., Kumari, A., Young, S. G., and Ploug, M. (2021) ANGPTL4 sensitizes lipoprotein lipase to PCSK3 cleavage by catalyzing its unfolding. *J. Lipid Res.* **62**, 100071
29. Chang, S. F., Reich, B., Brunzell, J. D., and Will, H. (1998) Detailed characterization of the binding site of the lipoprotein lipase-specific monoclonal antibody 5D2. *J. Lipid Res.* **39**, 2350–2359
30. Rønne, E., Behrendt, N., Ellis, V., Ploug, M., Danø, K., and Høyer-Hansen, G. (1991) Cell-induced potentiation of the plasminogen activation system is abolished by a monoclonal antibody that

≋ASBMB

recognizes the NH2-terminal domain of the urokinase receptor. *FEBS Lett.* **288**, 233–236

31. Gårdsvoll, H., Hansen, L. V., Jørgensen, T. J., and Ploug, M. (2007) A new tagging system for production of recombinant proteins in Drosophila S2 cells using the third domain of the urokinase receptor. *Protein Expr. Purif.* **52**, 384–394

32. Gårdsvoll, H., Werner, F., Søndergaard, L., Danø, K., and Ploug, M. (2004) Characterization of low-glycosylated forms of soluble human urokinase receptor expressed in Drosophila Schneider 2 cells after deletion of glycosylation-sites. *Protein Expr. Purif.* **34**, 284–295

33. Iverius, P. H., and Ostlund-Lindqvist, A. M. (1976) Lipoprotein lipase from bovine milk. Isolation procedure, chemical characterization, and molecular weight analysis. *J. Biol. Chem.* **251**, 7791–7795

34. Bengtsson, G., and Olivecrona, T. (1980) Lipoprotein lipase. Mechanism of product inhibition. *Eur. J. Biochem.* **106**, 557–562

35. Panteghini, M., Bonora, R., and Pagani, F. (2001) Measurement of pancreatic lipase activity in serum by a kinetic colorimetric assay using a new chromogenic substrate. *Ann. Clin. Biochem.* **38**, 365–370

36. Kristensen, K. K., Midtgaard, S. R., Mysling, S., Kovrov, O., Hansen, L. B., Skar-Gislinge, N., Beigneux, A. P., Kragelund, B. B., Olivecrona, G., Young, S. G., Jørgensen, T. J. D., Fong, L. G., and Ploug, M. (2018) A disordered acidic domain in GPIHBP1 harboring a sulfated tyrosine regulates lipoprotein lipase. *Proc. Natl. Acad. Sci. U.S.A.* **115**, E6020–E6029

37. Luz, J. G., Beigneux, A. P., Asamoto, D. K., He, C., Song, W., Allan, C. M., Morales, J., Tu, Y., Kwok, A., Cottle, T., Meiyappan, M., Fong, L. G., Kim, J. E., Ploug, M., Young, S. G., *et al.* (2020) The structural basis for monoclonal antibody 5D2 binding to the tryptophan-rich loop of lipoprotein lipase. *J. Lipid Res.* **61**, 1347–1359

38. Ghisaidoobe, A. B., and Chung, S. J. (2014) Intrinsic tryptophan fluorescence in the detection and analysis of proteins: A focus on förster resonance energy transfer techniques. *Int. J. Mol. Sci.* **15**, 22518–22538

39. Jin, W., Fuki, I. V., Seidah, N. G., Benjannet, S., Glick, J. M., and Rader, D. J. (2005) Proprotein convertases [corrected] are responsible for proteolysis and inactivation of endothelial lipase. *J. Biol. Chem.* **280**, 36551–36559

40. Kristensen, K. K., Leth-Espensen, K. Z., Mertens, H. D. T., Birrane, G., Meiyappan, M., Olivecrona, G., Jørgensen, T. J. D., Young, S. G., and Ploug, M. (2020) Unfolding of monomeric lipoprotein lipase by ANGPTL4: Insight into the regulation of plasma triglyceride metabolism. *Proc. Natl. Acad. Sci. U.S.A.* **117**, 4337–4346

41. Hahn, P. F. (1943) Abolishment of alimentary lipemia following injection of heparin. *Science.* **98**, 19–20

42. Havel, R. J., and Gordon, R. S. (1960) Idiopathic hyperlipemia: metabolic studies in an affected family. *J. Clin. Invest.* **39**, 1777–1790

43. Beigneux, A. P., Davies, B. S., Gin, P., Weinstein, M. M., Farber, E., Qiao, X., Peale, F., Bunting, S., Walzem, R. L., Wong, J. S., *et al.* (2007) Glycosylphosphatidylinositol-anchored high-density lipoprotein-binding protein 1 plays a critical role in the lipolytic processing of chylomicrons. *Cell Metab.* **5**, 279–291

44. Mysling, S., Kristensen, K. K., Larsson, M., Kovrov, O., Bensadouen, A., Jørgensen, T. J., Olivecrona, G., Young, S. G., and Ploug, M. (2016) The angiopoietin-like protein ANGPTL4 catalyzes unfolding of the hydrolase domain in lipoprotein lipase and the endothelial membrane protein GPIHBP1 counteracts this unfolding. *Elife.* **5**, e20958

45. Gunn, K. H., Roberts, B. S., Wang, F., Strauss, J. D., Borgnia, M. J., Egelman, E. H., and Neher, S. B. (2020) The structure of helical lipoprotein lipase reveals an unexpected twist in lipase storage. *Proc. Natl. Acad. Sci. U.S.A.* **117**, 10254–10264

46. Bengtsson-Olivecrona, G., and Olivecrona, T. (1985) Binding of active and inactive forms of lipoprotein lipase to heparin. Effects of pH. *Biochem. J.* **226**, 409–413

47. Zitzmann, J., Schreiber, C., Eichmann, J., Bilz, R. O., Salzig, D., Weidner, T., and Czermak, P. (2018) Single-cell cloning enables the selection of more productive Drosophila melanogaster S2 cells for recombinant protein expression. *Biotechnol. Rep. (Amst).* **19**, e00272